Hindawi
Advances in Civil Engineering
Volume 2023, Article ID 2862550, 8 pages
https://doi.org/10.1155/2023/2862550

Research Article

Inversion Study of Mechanical Parameters of Tunnel Surrounding Rock Based on Similar Test

Xianyun Wang, Hewei Cui, Hailiang Xu, Dong An, and Yimin Song

School of Civil Engineering, North China University of Technology, Beijing 100144, China

Correspondence should be addressed to Hewei Cui; 279805644@qq.com

Received 15 November 2022; Revised 19 December 2022; Accepted 3 January 2023; Published 19 January 2023

Academic Editor: Ma Jianjun

Based on similar model tests and finite element simulations, inversion study of the mechanical parameters of the tunnel surrounding rock by combining artificial fish swarm algorithm (AFSA) and digital scattering correlation method is carried out. The inversion of the mechanical parameters of the tunnel surrounding rock is carried out by iterating the optimization algorithm to minimize the objective function value through similar model test with the displacement measurements obtained by the digital scattering correlation method as the known quantity and the nodal displacement simulation values obtained by numerical simulation as the unknown quantity. The results show the following: (1) The new research idea proposed in this paper is effective and feasible and can perform the inversion calculation of the parameters of the soft and weak tunnel surrounding rock. (2) Through the inversion calculation, the parameters related to the surrounding rock show a wave-like change: the parameters increase in the initial and final compaction stages due to the small deformation rate of the tunnel and decrease in the continuous loading stage due to the increasing deformation rate of the tunnel. (3) The displacement field calculated by DSCM in the test is basically the same as the displacement distribution characteristics of the numerical simulation displacement cloud map, and the error of nodal displacement value is within 3%.

1. Introduction

Soft and weak surrounding rocks are characterized by low strength, poor self-stabilization, and easy to change shape, which are the riskiest and collapse-prone geological conditions during tunnel construction. According to 89 accidents occurred during tunnel construction from 2006–2016, 50.6% of which were collapses caused by soft surrounding rocks [1]. Tunnel excavation is a dynamic process, with the progress of excavation work, the tunnel surrounding rock parameters are changing in time and space, especially the weak envelope parameters change more significantly. Therefore, it is necessary to optimize the excavation method and support scheme according to the changes of rock parameters during the construction process to avoid accidents. Therefore, how to provide real-time feedback on the change of rock parameters and predict the deformation and force of the surrounding rock during the construction stage is the main problem faced by the research now.

A large number of scholars have carried out research work on theoretical aspects of rock masses and numerical simulations [2–7]. The inversion method using a combination of actual measurements and numerical calculations is one of the effective methods to obtain the mechanical parameters of the surrounding rocks. Zhang et al. [8] relied on the field data, with the aid of Midas numerical simulation and the nonlinear mapping capability of BP neural network, to invert the mechanical parameters of fractured and weak surrounding rocks traversed in the section. Based on the displacement measurement of the soft body impact of aluminum plate, Yu et al. [9] used BP neural network to invert the bird composition model and showed that the proposed inversion model is more reasonable. Cao et al. [10] improved the accuracy of inversion of modulus of each structural layer of asphalt by layer-by-layer inversion method to provide a basis for research. Luo et al. [11] used the measured data, combined with GA-BP neural network, to calculate the mechanical parameters of the surrounding

rock by displacement inverse analysis method. Gu et al. [12] using the measured displacement data and Bayesian inverse analysis theory, an inversion method of the mechanical parameters of concrete dams was proposed and the stochastic properties of concrete dams were inverted. Wang et al. [13] taking the Lanzhou-Haikou tunnel as an engineering example, the inversion analysis method of IA-BP algorithm was used to perform multiparameter creep inversion of the tunnel surrounding rock under the stress-percolation coupling conditions. Chen et al. [14] used the particle swarm optimization (PSOGSA-SVM) method of support vector machine gravity search algorithm to invert the elastic modulus of the high arch dam partition based on the deformation safety monitoring data during the operation period. Wang et al. [15] combined the field monitoring data and FLAC3D finite element software to perform displacement inversion analysis and tunnel numerical simulation calculations for the surrounding rock loosening area. Yang et al. [16] combined digital image correlation techniques and finite element simulation to invert the parameters of automotive composites. Hou et al. [17], combined with D-InSAR monitoring technology, used inversion method to inverse IPIM-G dynamic prediction model parameters for mining subsidence prediction. Xiong et al. [18], combined with DNN (deep neural network), analyzed the sensitivity of seismic attributes to rock mechanics parameters to realize parameter inversion. Liu et al. [19], according to the finite element theory, proposed a displacement inverse model for solving the elastic modulus of each rock layer of the underground roadway based on the measured displacement after excavation of the underground roadway in coal mines. Liu et al. [20] used the measured vault settlement, peripheral displacement, and surface settlement values of the cross section and input them into the well-trained GA-BP neural network model, and the output obtained parameters such as elastic modulus, Poisson's ratio, cohesion, and internal friction angle of the surrounding rock. Based on the surface settlement monitoring data during the actual tunnel construction, Ruan et al. [21] used POS-SVM to invert the compression modulus of the reinforced peaty soil and clay layers around the tunnel.

Due to the complicated burial process, limited test points, and the influence of multiple factors such as burial location and depth, the inversion of the surrounding rock parameters cannot meet the expected requirements. To address the shortcomings of the existing research methods, this paper established a new research idea: to establish similar model experiments according to the actual geological conditions, to bring the displacement measurement values obtained from similar model test measurements and displacement simulation values obtained from numerical simulation into the objective function, to minimize the value of the objective function through the optimization algorithm, and to obtain the mechanical parameters of the similar model surrounding rock and the evolution of the parameters with the excavation process by inversion calculation. The inversion calculation is carried out to obtain the mechanical parameters of the similar model surrounding rock and the evolution law of the parameters with the excavation process.

2. Inversion Process

Similar model test is established with the background of actual geological conditions of a project. The test uses the digital scatter correlation method [22–25] (DSCM) to obtain the displacement values of the measured area deformed with tunnel excavation as the known quantities in the inversion method. The simulated values of model node displacements are calculated by the optimization algorithm [26] (AFSA) randomly assigned to the material parameters of the ABAQUS finite element model as the unknown quantity in the inversion equation, and the measured and simulated values are brought into the objective function to obtain the corresponding function values. The function values are minimized by continuous iterative calculations of the optimization algorithm, and the mechanical parameters of the surrounding rock are derived. The calculation flow is shown in Figure 1.

3. Indoor Similar Model Tests

3.1. Test Principle and Material Parameters. According to the similarity principle [27], material parameters such as modulus of elasticity, Poisson's ratio, and other parameters in the similarity test need to satisfy the following relationships:

$$C_\mu = 1, \tag{1}$$

$$\frac{C_\gamma C_L}{C_\sigma} = 1, \tag{2}$$

$$C_E = C_C = C_\sigma = 1. \tag{3}$$

In the formula, C_μ is Poisson's ratio similar ratio, C_E is modulus of elasticity similar ratio, C_C is cohesive similarity ratio, C_γ is volume to weight ratio, C_σ is stress similarity ratio, and C_L is geometric similarity ratio.

The geometric similarity ratio is selected as 100 according to the dimensions of the model stand. The similarity ratio for each parameter according to the above equation is as follows: weight capacity $C_\gamma = 1$; Poisson's ratio $C_\mu = 1$; stress, cohesion, and modulus of elasticity $C_C = C_\sigma = C_E = 100$.

In this test, the IV surrounding rock was used as the main research subject, and referring to the existing literature [28–30], barite, gypsum, quartz sand, detergent, and water were selected as similar materials to simulate the tunnel surrounding rock, and the material ratio was barite: quartz sand: gypsum: detergent: water = 12 : 4 : 2 : 1 : 1. The parameters of IV surrounding rock and similar materials are shown in Table 1.

3.2. Test Model. The test consists of two systems: loading and monitoring. The loading system uses a multichannel electrohydraulic servo similar model material test stand, which can be loaded horizontally and vertically in both directions, with a maximum loading capacity of 0.8 MPa and a stand model size of $1.2 \times 1.2 \times 0.3$ m. The tunnel is simplified as a circular

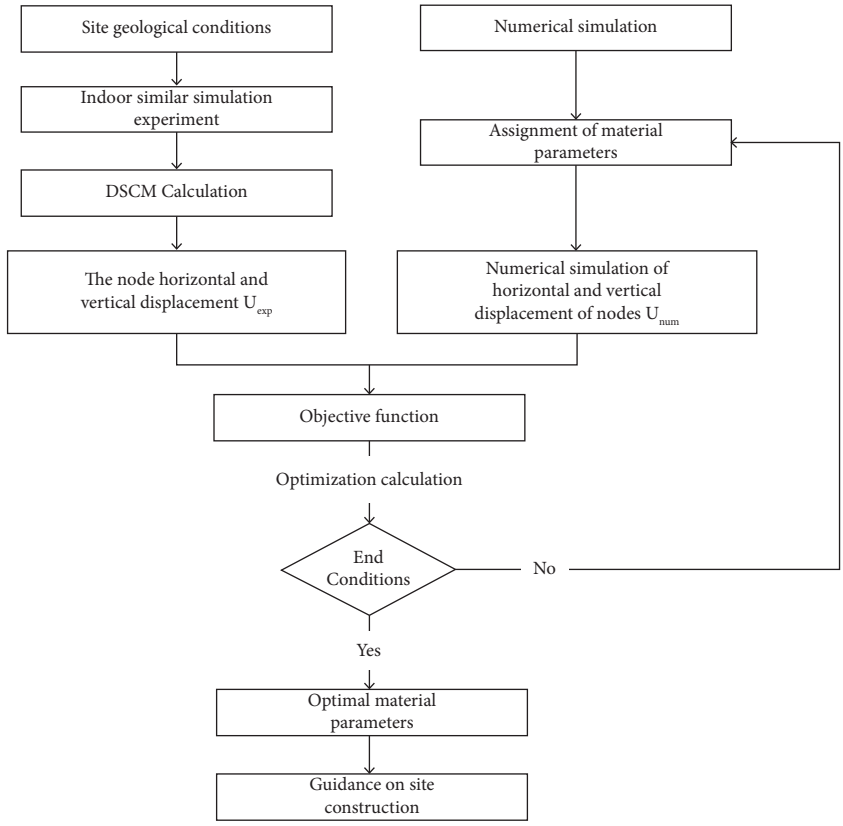

Figure 1: Computational flow.

Table 1: Material parameters.

Materials	Weight capacity ($kN \cdot m^{-3}$)	Modulus of elasticity (MPa)	Cohesion (kPa)	Poisson's ratio	Internal friction angle (°)
IV perimeter rock	20	5000	1600	0.3	31
Similar materials	20	50	16	0.3	31

chamber placed in the center of the model with a diameter of $D = 0.15$ m as shown in Figure 2.

The monitoring system adopts the digital scatter correlation method, spraying 0.45×0.45 m black and white scatter points as the monitoring area with the tunnel as the center, and the monitoring system is composed by the loading system, CCD camera, and computer. CCD camera acquisition rate was of 1 frame/s, image resolution of 1600×1200 pixels, and object surface resolution of 0.55 mm/pixel. The final test system is shown in Figure 3.

3.3. Test and Result Calculation. The test sequence was "opening the hole first and then loading," through the model top vertical steady loading, to simulate the internal stress changes and local stress concentration of the surrounding rock caused by the tunnel excavation. The deformation process and damage law of the surrounding rock during tunnel excavation were analyzed and studied with the tunnel section as the research object. The test loading was controlled by pressure, and the top plate of the table was loaded downward at a loading rate of 10 kN/min, while the bottom plate and side plates of the table were fixed. In this paper, three moments of 10 kN, 20 kN, and 30 kN pressure were selected for calculation and analysis.

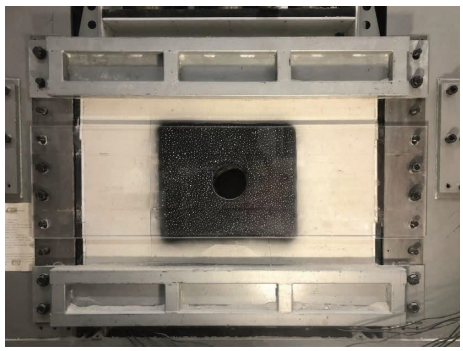

Figure 2: Surface of experimental model.

We used the scatter image taken at $t = 0$ as the reference image and the scatter images at the pressure of 10 kN, 20 kN, and 30 kN as the target images. Through DSCM data processing, the horizontal and vertical displacement fields of the

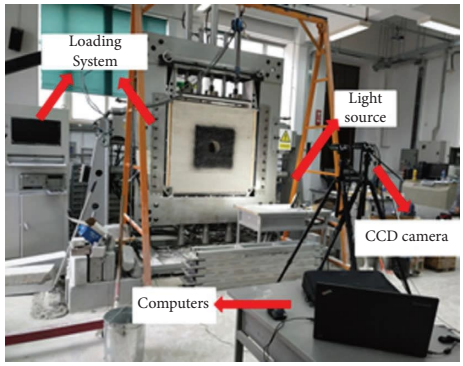

Figure 3: Experimental system.

measurement area at three moments during the test are shown in Figures 4 and 5, and the displacement measurement values at three moments are shown in Table 2.

From Figures 4 and 5 and Table 2, it can be seen that the horizontal displacement field of the tunnel surrounding rock is symmetrically distributed, the overall expansion trend on both sides of the tunnel level, the maximum horizontal displacement is distributed in the horizontal left and right sides of the cavity. As the pressure increases, the displacement field distribution does not change significantly, and the horizontal displacement gradually increases, the maximum horizontal displacement is 0.22 mm, 0.54 mm, and 1.13 mm, respectively. During the test process, the overall settlement of the model compression tunnel occurs. The vertical displacement at the top is greater than that at the bottom, and the overall tunnel shows an inward shrinkage trend. As the pressure increases, the displacement field distribution does not change significantly, and the vertical displacement gradually increases, with the maximum vertical displacement of 1.36 mm, 4.88 mm, and 9.22 mm, respectively.

4. Inversion Calculation

4.1. Numerical Modeling. The model was established using ABAQUS finite element software as shown in Figure 6. The model size was $1.2 \times 1.2 \times 0.3$ m, and the tunnel was located in the center of the model with diameter $D = 0.15$ m. The grid cell type was C3D8, and the grid of the measurement area in the test was encrypted to correspond to the red area in Figure 6, with 620 nodes. The bottom end of the model was fixed, the x-direction displacement was constrained on both sides, and the z-direction displacement was constrained at the front and rear of the model, and 10 kN, 20 kN, and 30 kN loads were applied at the top of the model.

4.2. Determination of the Objective Function. The objective function formula was used as follows [31]:

$$Q(P) = \sqrt{\sum_{i=1}^{m} (S_i(p) - M_i)^2}. \quad (4)$$

In the formula, m is the number of data points, P is the unknown mechanical parameter of the material, S_i is the numerical calculation data, and M_i is the experimental measurement data.

The displacement data obtained from the finite element numerical calculation and similar model test calculation are used as S_i and M_i in equation (4), and the inverse parameters are used as the unknown quantity P to establish the objective function as follows:

$$Q(P) = \sqrt{\sum_{i=1}^{m} \left(U_{i,x}^{\text{num}} - U_{i,x}^{\text{exp}}\right)^2 + \sum_{i=1}^{m} \left(U_{i,y}^{\text{num}} - U_{i,y}^{\text{exp}}\right)^2}. \quad (5)$$

4.3. Parameter Inversion Calculation. The inversion calculation takes the displacement field at the moments of 10 kN, 20 kN, and 30 kN pressure as the inversion object, and the inversion calculation was performed by ABAQUS model corresponding to 620 nodes in the scattered area, and some of the interpolated displacement of the scattered nodes are shown in Table 3.

The calculation has set the number of fish in the fish swarm optimization algorithm to 4, the number of iterations to 40, the elastic modulus calculation range to 55~45 MPa, the cohesion calculation range to 10~30 kPa, Poisson's ratio calculation range to 0.2~0.4, and the internal friction angle calculation range to 20~40°, and the calculation results are shown in Table 4.

From Table 4, it can be seen that the surrounding rock parameters show an overall change trend of increasing then decreasing and finally increasing again. Taking the elastic modulus E as an example, the elastic modulus increases from 50 MPa to 50.70 MPa in the 0~10 kN loading stage, which is the initial loading stage, the tunnel deformation rate is low, and the compaction of similar materials dominates, so the phenomenon of increasing the mechanical parameters related to the surrounding rock appears in this stage. The elastic modulus decreases from 50.70 MPa to 49.97 MPa in the 10~20 kN loading stage, this stage is the continuous loading stage, the tunnel deformation rate increases, and the tunnel deformation release dominates, so the mechanical parameters of surrounding rock decreases; 20–30 kN loading stage, this stage is the final compaction stage, as the tunnel deformation stabilizes, the tunnel deformation rate decreases, the elastic modulus increases from 49.97 MPa to 50.79 MPa, so the mechanical parameters of surrounding rock increases. Other inversion parameters and elastic modulus show the same trend.

From the above analysis, it can be seen that the mechanical parameters related to the soft tunnel surrounding rock are affected by multiple factors such as loading conditions, excavation area, and surrounding rock deformation, and the trend of change is more complicated. This inversion idea can accurately calculate the surrounding rock parameters from the surrounding rock deformation data around the tunnel, which can play a certain guiding role for the construction site.

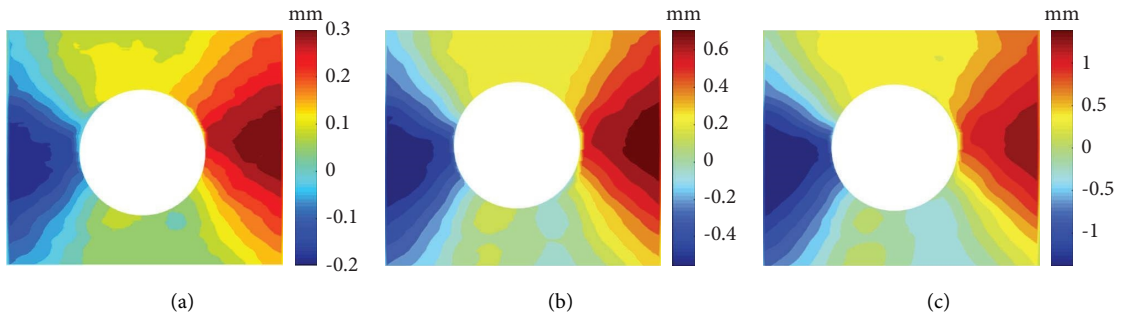

Figure 4: Horizontal displacement field. (a) 10 kN. (b) 20 kN. (c) 30 kN.

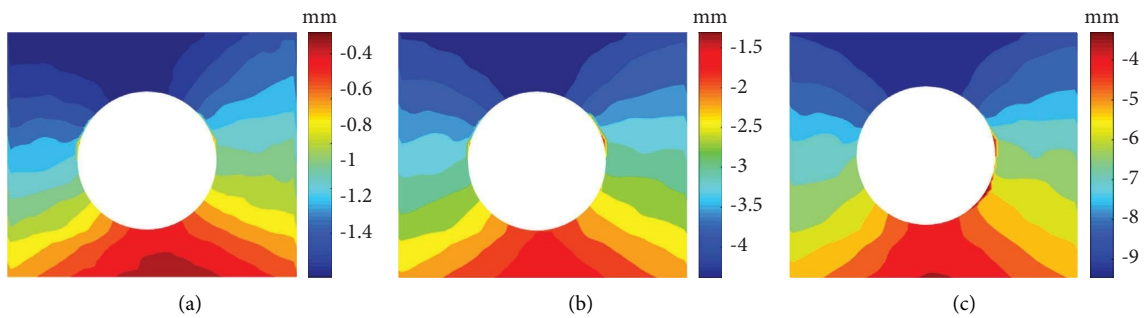

Figure 5: Vertical displacement field. (a) 10 kN. (b) 20 kN. (c) 30 kN.

Table 2: Experimental displacement.

Vertical load (kN)	Horizontal displacement (mm)	Vertical displacement (mm)
10	−0.22~0.22	−0.35~−1.36
20	−0.53~0.54	−1.33~−4.88
30	−1.12~1.13	−3.21~−9.22

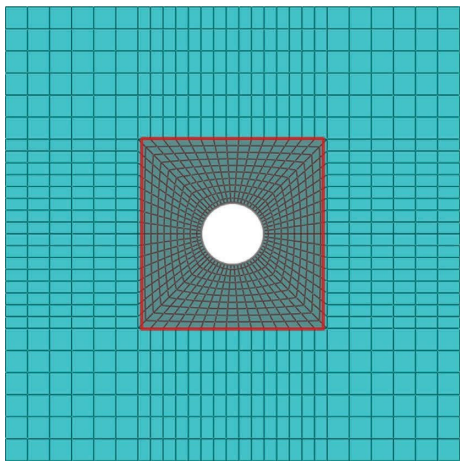

Figure 6: Computational model.

4.4. Numerical Simulation, Calculation, and Validation. In order to verify the accuracy of the inversion parameters, the parameters obtained from the inversion calculations were carried back into the numerical model, and the simulation calculation results were compared with the measured results for verification. By applying 10 kN, 20 kN, and 30 kN vertical loads, respectively, the displacement clouds of the model surface are calculated by static analysis, as shown in Figures 7 and 8.

Table 3: Interpolation displacements of some speckle nodes.

Node number	x (mm)	y (mm)	U_x (mm)	U_y (mm)
104	345	315	0.111	1.423
105	375	315	0.150	1.438
106	405	315	0.146	1.417
107	435	315	0.102	1.355
108	465	315	0.120	1.320
109	495	315	0.160	1.290
110	525	315	0.202	1.295
111	555	315	0.197	1.249
112	585	315	−0.015	1.384
113	615	315	−0.028	1.380
114	645	315	−0.0129	1.348

From Figure 7, it can be seen that the horizontal displacement field of the model is symmetrically distributed, the tunnel shows an overall trend of expansion on both horizontal sides. From Figure 8, it can be seen that the tunnel as a whole is settling, and the vertical displacement at the top of the model is larger than the

Table 4: Parameter inversion results.

Vertical load (kN)	Modulus of elasticity (MPa)	Amount of change	Cohesion (kPa)	Amount of change	Poisson's ratio	Amount of change	Angle of internal friction (°)	Amount of change
0	50	—	16	—	0.3	—	31	—
10	50.70	+1.40%	18.01	+12.56%	0.29	−3.33%	31.03	+0.01%
20	49.97	−0.06%	14.87	−7.06%	0.27	−10.00%	31.42	+1.35%
30	50.79	+1.58%	17.66	+10.38%	0.31	+3.33%	29.29	−5.52%

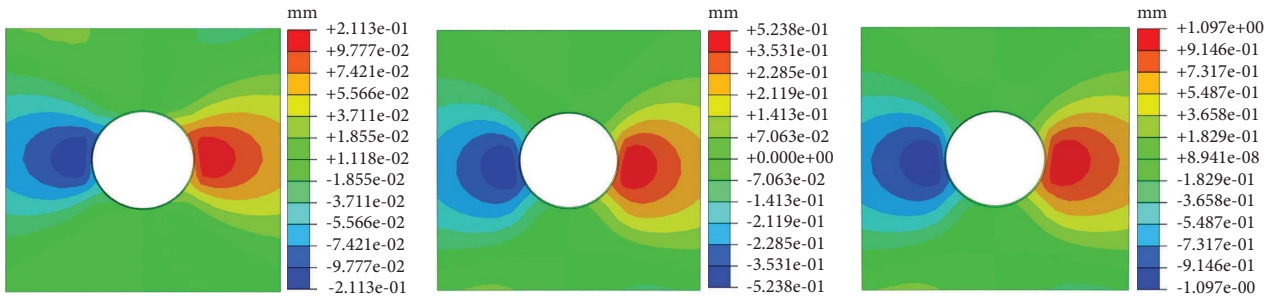

Figure 7: Horizontal displacement cloud map. (a) 10 kN. (b) 20 kN. (c) 30 kN.

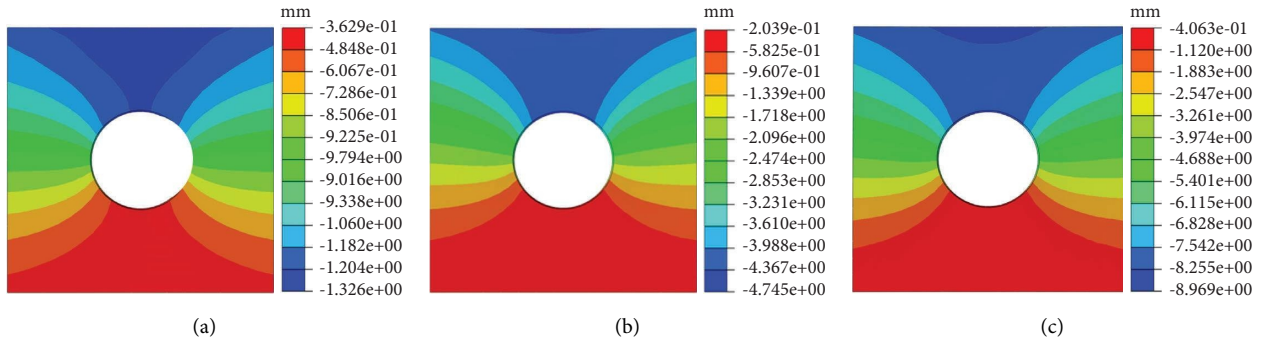

Figure 8: Vertical displacement cloud map. (a) 10 kN. (b) 20 kN. (c) 30 kN.

vertical displacement at the bottom, and the tunnel is inwardly shrinking. As the pressure increases, the displacement field distribution does not change significantly, and the horizontal and vertical displacements gradually increases. The numerical simulation results are similar to the DSCM calculation results.

From the above analysis, it can be seen that the displacement field distribution characteristics of similar test results and numerical simulation results are basically the same, and the displacement value error is within 3%. In a comprehensive view, the mechanical parameters obtained from the inversion are more satisfactory.

5. Conclusion

(1) The inversion calculation idea of tunnel surrounding rock mechanical parameters based on similar model test and ABAQUS finite element simulation established in this paper can be carried out effectively by combining artificial fish swarm algorithm (AFSA) with digital scattering correlation method.

(2) The comparison between the inversion calculation results and the initial surrounding rock parameters shows that the surrounding rock related parameters show a general trend of increasing then decreasing and finally increasing again: the tunnel deformation rate is low in the initial stage of loading, the compaction of similar materials dominates, and the surrounding rock related mechanical parameters increase. The tunnel deformation rate increases in the continuous loading stage, the tunnel deformation release dominates and the surrounding rock related mechanical parameters decrease. The final compaction stage tunnel deformation tends to stabilize, the deformation rate decreases, so the mechanical parameters related to the surrounding rock appears to increase.

(3) The displacement field calculated by DSCM in the test is basically the same as the displacement distribution characteristics of the numerical simulation displacement cloud map, and the displacement value has error, the error is within 3%.

In summary, the mechanical parameters obtained by the inversion calculation are ideal, and the feasibility of the calculation method is verified, and it has good engineering application value.

Data Availability

The data that support the findings of this study are available from the corresponding author upon reasonable request.

Conflicts of Interest

The authors declare that they have no conflicts of interest.

Acknowledgments

This work was supported by the National Natural Science Foundation of China (51774015).

References

[1] J. W. Zhang, Y. Y. Chen, T. Chen et al., "Law and characteristics analysis of domestic tunnel construction accidents from 2006 to 2016," *Chinese Journal of Modern Tunnelling Technology*, vol. 55, no. 3, pp. 10–17, 2018.

[2] L. C. Huang, J. G. Liang, J. J. Ma, and W Chen, "A dynamic bounding surface plasticity damage model for rocks subjected to high strain rates and confinements," *International Journal of Impact Engineering*, vol. 168, Article ID 104306, 2022.

[3] L. C. Huang, J. G. Liang, J. J. Ma, H. Yang, and Y. Gui, "Spherical cavity expansion in porous rock considering plasticity and damage," *International Journal for Numerical and Analytical Methods in Geomechanics*, vol. 45, no. 15, pp. 2235–2259, 2021.

[4] J. J. Ma, J. J. Chen, W. Chen, and L. Huang, "A coupled thermal-elastic-plastic-damage model for concrete subjected to dynamic loading," *International Journal of Plasticity*, vol. 153, Article ID 103279, 2022.

[5] J. J. Ma, G. F. Zhao, and N. Khalili, "An elastoplastic damage model for fractured porous media," *Mechanics of Materials*, vol. 100, pp. 41–54, 2016.

[6] J. J. Ma, P. J. Yin, L. C. Huang, and Y. Liang, "The application of distinct lattice spring model to zonal disintegration within deep rock masses," *Tunnelling and Underground Space Technology*, vol. 90, pp. 144–161, 2019.

[7] J. J. Ma, J. J. Chen, J. W. Guan, Y. Lin, W. Chen, and L. Huang, "Implementation of Johnson-Holmquist-Beissel model in four-dimensional lattice spring model and its application in projectile penetration," *International Journal of Impact Engineering*, vol. 170, Article ID 104340, 2022.

[8] Q. B. Zhang, J. C. Li, and J. P. Xu, "Back analysis of surrounding rock parameters of fractured soft rock tunnel," *Chinese Journal of Highway*, vol. 64, no. 12, pp. 293–297, 2019.

[9] P. Yu, S. L. Yu, S. He, X. Huang, and W Yun, "Inversion for constitutive model parameters of bird in case of bird striking," *Shock and Vibration*, vol. 2022, pp. 1–10, 2022.

[10] M. M. Cao, W. Q. Huang, Y. W. Zou, and G. Liu, "Modulus inversion layer by layer of different asphalt pavement structures," *Advances in Civil Engineering*, vol. 2021, pp. 1–10, 2021.

[11] A. Z. Luo, H. S. Qiu, J. Xiong, and Z. Y. Zhou, "Back analysis of mechanical parameters of soft rock tunnel surrounding rock based on GA-BP neural network," *Chinese Journal of Engineering and Construction*, vol. 34, no. 5, pp. 920–922, 2020.

[12] C. S. Gu, X. Cao, and B. Xu, "Stochastic inversion method for concrete dams on the basis of bayesian back analysis theory," *Advances in Civil Engineering*, vol. 2019, Article ID 5943913, 13 pages, 2019.

[13] J. X. Wang, J. Sun, H. J. Kou, and Y. Lin, "Multiparameter inversion early warning system of tunnel stress-seepage coupling based on IA-BP algorithm," *Advances in Civil Engineering*, vol. 2021, Article ID 1566693, 19 pages, 2021.

[14] B. Chen, X. Fu, XY. Guo, C. Gu, C. Shao, and X. Qin, "Zoning elastic modulus inversion for high arch dams based on the PSOGSA-SVM method," *Advances in Civil Engineering*, vol. 2019, Article ID 7936513, 13 pages, 2019.

[15] H. Wang, J. M. Li, J. M. Wu, J. Zhang, and R. Q. Li, "Inverse analysis on mechanical parameters of soft rock mass around shallow buried large-section hydraulic tunnel," *Chinese Journal of Geotechnical Investigation & Surveying*, vol. 48, no. 4, pp. 1–5, 2020.

[16] S. M. Yang, C. Jiang, and B. Y. Ni, "An parameter estimation method of composite used in vehicle based on DIC technique," *Chinese Journal of Mechanical Science and Technology for Aerospace Engineering*, vol. 35, no. 12, pp. 1944–1949, 2016.

[17] Z. X. Hou, K. M. Yang, Y. R. Li et al., "Dynamic prediction model of mining subsidence combined with D-InSAR technical parameter inversion," *Environmental Earth Sciences*, vol. 81, no. 11, p. 307, 2022.

[18] F. S. Xiong, H. Yong, H. Chen, H. Wang, and W. Shen, "Biot's equations-based reservoir parameter inversion using deep neural networks," *Journal of Geophysics and Engineering*, vol. 18, no. 6, pp. 862–874, 2021.

[19] Y. J. Liu, Y. Liu, and D. W. Zheng, "Optimization algorithm in the back analysis of mechanical parameters from displacements," *Chinese Journal of Journal*, of Liaoning Technical University, no. 2, pp. 142–144, 2000.

[20] J. Liu, X. J. Weng, L. S. Zhang, and L. Z. Zhang, "Inversion of mechanical parameters of tunnel surrounding rock based on GA-BP neural network," *Chinese Journal of Journal of Highway and Transportation Research and Development*, vol. 37, no. 7, pp. 90–96, 2020.

[21] Y. F. Ruan, D. X. Yu, J. Yang, L. Wu, and G. P. Tan, "Inversion of mechanical parameters of reinforced soft soil around tunnel based on PSO-svm," *Chinese Journal of Journal of Highway and Transportation Research and Development*, vol. 37, no. 6, pp. 87–96, 2020.

[22] I. Yamaguchi, "A Laser-speckle strain gauge," *Journal of Physics E: Scientific Instruments*, vol. 14, no. 11, pp. 1270–1273, 1981.

[23] W. H. Peters and W. F. Ranson, "Digital imaging techniques in experimental stress analysis," *Optical Engineering*, vol. 21, no. 3, Article ID 213427, 1982.

[24] G. L. Liu and H. Y. Jiang, "Principle of digital speckle correlation method and its applications in civil engineering deformation measurement," *Chinese Journal of Journal of Anhui Jianzhu University*, vol. 23, no. 6, pp. 52–58, 2015.

[25] B. Pan, H. M. Xie, and F. L. Dai, "An investigation of sub-pixel displacements registration algorithms in digital image

correlation," *Chinese Journal of Chinese Journal of Theoretical and Applied Mechanic*, vol. 2, pp. 245–252, 2007.

[26] X. L. Li, *A Novel Intelligent Optimization Method-Artificial Fish Swarm Algorithmm*, Zhejiang University, Zhejiang, China, 2003.

[27] M. F. Wan, *Research on Mechanical Behavior of Excavation in Super-large Span Highway Tunnel*, Northeastern University, Northeastern, MA, 2009.

[28] B. T. Wu, H. H. Zhu, Q. W. Xu, and J. Ming, "Experimental study of similar material for weak surrounding rock mass of class IV," *Chinese Journal of Rock and Soil Mechanics*, vol. 34, no. S1, pp. 109–116, 2013.

[29] B. L. Han, X. L. Chen, Y. L. Song, and H. M. Li, "Research on similar material of rockmass," *Chinese Journal of Engineering Journal of Wuhan University*, no. 2, pp. 7–10, 1997.

[30] C. B. Wang, H. H. Zhu, and H. L. Wang, "Model test study on failure mechanism of unsupported tunnels constructed in soft rock masses at different cross section," *Applied Mechanics and Materials*, vol. 90-93, pp. 2282–2285, 2011.

[31] Y. J. Xu, Y. Q. Guo, L. H. Liang, Y. Liu, and X. Wang, "A unified cohesive zone model for simulating adhesive failure of composite structures and its parameter identification," *Composite Structures*, vol. 182, pp. 555–565, 2017.